


An Extreme Learning Machine-Based Neuromorphic Tactile Sensing System for Texture Recognition

Mahdi Rasouli , *Student Member, IEEE*, Yi Chen, *Member, IEEE*, Arindam Basu, *Member, IEEE*,
Sunil L. Kukreja, *Senior Member, IEEE*, and Nitish V. Thakor, *Fellow, IEEE*

Abstract—Despite significant advances in computational algorithms and development of tactile sensors, artificial tactile sensing is strikingly less efficient and capable than the human tactile perception. Inspired by efficiency of biological systems, we aim to develop a neuromorphic system for tactile pattern recognition. We particularly target texture recognition as it is one of the most necessary and challenging tasks for artificial sensory systems. Our system consists of a piezoresistive fabric material as the sensor to emulate skin, an interface that produces spike patterns to mimic neural signals from mechanoreceptors, and an extreme learning machine (ELM) chip to analyze spiking activity. Benefiting from intrinsic advantages of biologically inspired event-driven systems and massively parallel and energy-efficient processing capabilities of the ELM chip, the proposed architecture offers a fast and energy-efficient alternative for processing tactile information. Moreover, it provides the opportunity for the development of low-cost tactile modules for large-area applications by integration of sensors and processing circuits. We demonstrate the recognition capability of our system in a texture discrimination task, where it achieves a classification accuracy of 92% for categorization of ten graded textures. Our results confirm that there exists a tradeoff between response time and classification accuracy (and information transfer rate). A faster decision can be achieved at early time steps or by using a shorter time window. This, however, results in deterioration of the classification accuracy and information transfer rate. We further observe that there exists a tradeoff between the classification accuracy and the input spike rate (and thus energy consumption). Our work substantiates the importance of development of efficient sparse codes for encoding sensory data to improve the energy efficiency. These results have a significance for a wide range of wearable, robotic, prosthetic, and industrial applications.

Index Terms—Extreme learning machine, neuromorphic, pattern recognition, tactile perception, texture.

I. INTRODUCTION

SKIN is an important sensory organ that shapes our interaction with the world. Electronic devices that recreate properties of the skin, also known as e-skins [1], have important applications in prosthetics [2] and robotics [3]. E-skin provides a robot or human user with advanced capabilities to enhance interactions with their environment [1]. One of the most important functions of skin is the sense of touch, which is one of our five essential senses of perception. Tactile perception is primarily used to understand characteristic properties about the surrounding environment or objects. These effects include texture, stiffness, roughness, and smoothness [4]. Our goal is to develop an e-skin that is capable of sensing and characterizing tactile stimuli. Particularly, we target texture discrimination because it is one of the most necessary and challenging tasks for artificial sensory systems [5], [6]. Table I lists some of existing literature on tactile-based texture recognition.

Artificial tactile sensing has been the subject of intensive research over the past few decades [16]–[18]. A wide variety of materials, devices, and manufacturing techniques have been investigated for fabrication of tactile sensors [18], [19]. Various algorithms for processing of tactile information have been also explored. These include support vector machine (SVM) [20], linear discriminant analysis (LDA) [10], k-nearest neighbors (kNN) [21], spiking neural network (SNN) [6], ELM [22], and Bayesian analysis [23]. These efforts have lead to development of sensory systems that have been used in a variety of tactile recognition tasks, including texture [24], stiffness [25], curvature [26], shape [27], and object classification [22]. [28] presents a recent review on tactile object recognition, including texture discrimination.

Although considerable advances have been made for tactile perception, existing devices are strikingly less efficient and capable than the human sensory system [29]. Humans are able to process a wide variety of sensory information rapidly and effortlessly, while expending several orders of magnitude less energy compared to the current state-of-the-art artificial systems [29], [30].

Inspired by the efficiency of biological systems, our goal is to develop a neuromorphic approach for tactile sensing. Neuromorphic systems aim to bridge the efficiency gap between

Manuscript received October 22, 2017; revised January 6, 2018; accepted January 10, 2018. Date of publication March 13, 2018; date of current version March 22, 2018. This work was supported by the Office of Naval Research, Arlington, VA, USA, under Grant NICOP N62909-15-1-2024. This paper was recommended by Associate Editor S. Ostadabbas. (*Corresponding author: Mahdi Rasouli.*)

M. Rasouli is with the Graduate School for Integrative Sciences and Engineering, National University of Singapore, Singapore 117456, and also with Singapore Institute for Neurotechnology (SINAPSE), National University of Singapore, Singapore 117456 (e-mail: rasouli@u.nus.edu).

Y. Chen and A. Basu are with the Centre of Excellence in IC Design (VIRTUS), Department of Electrical and Electronics Engineering, Nanyang Technological University, Singapore 117456 (e-mail: chenyl@ntu.edu.sg; arindam.basu@ntu.edu.sg).

S. L. Kukreja is with Singapore Institute for Neurotechnology (SINAPSE), National University of Singapore, Singapore 117456 (e-mail: sunilkukreja.sinapse@gmail.com).

N. V. Thakor is with Singapore Institute for Neurotechnology (SINAPSE), National University of Singapore, Singapore 117456, and also with Johns Hopkins University, Baltimore, MD 21218 USA (e-mail: sinapsedirector@gmail.com).

Color versions of one or more of the figures in this paper are available online at <http://ieeexplore.ieee.org>.

Digital Object Identifier 10.1109/TBCAS.2018.2805721

TABLE I
SOME OF EXISTING WORK ON TACTILE-BASED TEXTURE RECOGNITION

Reference	Sensor Type	Signal Type	Features used	Analytical Method	Embedded Processing?	Spike-Based?
[7]	Piezoelectric (PVDF)	Spatiotemporal spike patterns (converted using the Izhikevich neuron model)	Spike timing	Spike train distance-based kNN	No	Yes
[8]	2 × 2 array of MEMS-based piezoresistive sensors	Spatiotemporal spike patterns (converted using the Izhikevich neuron model)	Spike timing	Interspike interval (ISI) statistics and spike distance metrics	No	Yes
[6]	Piezoelectric (PVDF)	Spatiotemporal spike patterns (converted using the Izhikevich neuron model)	Nonlinear frequency information extracted from the spike trains using bandpass filtering	Recurrent spiking neural network	No	Yes
[9]	Resistive sensor based on single layer graphene	Analogue sensor output	Fast Fourier Transform (FTT) spectrum	Analysis of FFT spectrum	No	No
[10]	Resistive MEMS tactile sensor	Analogue sensor output	Features extracted from grayscale and binary tactile images	SVM, kNN, and linear discriminant analysis	No	No
[11]	Optical tactile sensor [12]	Analogue sensor output	Surface geometry from tactile images	Multi-scale local binary pattern (MLBP) analysis	No	No
[13], [14]	Strain gauge & PVDF films	Analogue sensor output	Fourier frequency coefficients	Naive Bayes classifier	No	No
[15]	Tri-axis hall effect sensor	Analogue sensor output	Time and frequency domain signals	Template based classification	No	No

artificial systems and their biological counterparts by emulating spiking neural mechanisms observed in nature [29], [30]. These systems utilize a new form of asynchronous output representation that carries timing information similar to spikes in the nervous systems [31]. Using such a representation, it is possible to achieve higher efficiencies through event-driven processing of information and reducing processing and transmission of redundant data. [32]. This feature has stimulated significant interest for the development of neuromorphic sensors and computing architectures [32].

Although neuromorphic visual and auditory sensory systems have been widely investigated over the past two decades [33]–[35], neuromorphic tactile perception has received minimal attention [3]. [36] developed a neuromorphic vibrotactile sensory system that imitates rat whiskers to enable a robot to actively explore and navigate its environment. This system implemented a hardware processing architecture to model large networks of leaky integrate-and-fire neurons to process vibrotactile information [37], [38]. Kim [39], [40] explored modeling mechanoreceptors found in glabrous skin for robotic and prosthetic applications. Bologna [41] studied decoding braille patterns from primary and secondary neurons in a two-layer network. They converted the output of a force sensor array to spikes using a leaky integrate-and-fire neuron model [41]. Similar neuromorphic approaches have been investigated to characterize surface properties [42] and incipient tactile stimulus [26] using the Izhikevich neuron model.

The feasibility of recognizing texture using neuromorphic techniques was recently demonstrated by Rongala *et al.* [8]. In their work, the outputs of a tactile array were converted to spikes using an Izhikevich neuron model then used to demonstrate that statistics of inter-spike intervals and the Victor Purpura (VP) distance between spike trains can be used for classification of ten naturalistic textures. Although their results confirmed the

importance of spike timing for texture classification, computation of the metrics require offline processing for the entire time window and, therefore, cannot be implemented in real-time. Friedl *et al.* [6] proposed a spiking neural network architecture to overcome this limitation. They deployed the neural engineering framework (NEF) [43] to convert sensor data into spike patterns using a heterogeneous population of neurons. This activity was then convolved by a hidden layer using bandpass filters to extract nonlinear frequency information. The resulting high-dimensional feature representation was classified using a neurally implemented support vector machine. Although the proposed network could be simulated on neuromorphic hardware such as SpiNNaker [44], it was only software based and was not implemented and tested on any neuromorphic hardware platforms. Moreover, its task-specific architecture could limit its application in a wide variety of pattern recognition tasks. Zhengkun *et al.* [7] also investigated possibility of using spiking data for classification of surface roughness which is closely related to texture recognition. They converted outputs of polyvinylidene difluoride (PVDF) tactile sensors to spike trains using the Izhikevich neuron model, and applied two kNN-based decoding schemes (in both spike feature space and spike train space) for surface roughness discrimination. Although usefulness of a learning mechanism was demonstrated in their work, it was only software based and suffered from lack of hardware implementation.

In this paper, we present a hardware-based neuromorphic system to overcome these shortcomings. Our system provides a platform which is capable of real-time processing of tactile information and learning different tasks by integrating the decoding algorithm with the sensing device. Such an architecture provides the opportunity for local processing of information, and thus, can help reduce the amount of data that need to be transmitted to the central processing unit. This helps achieve portable

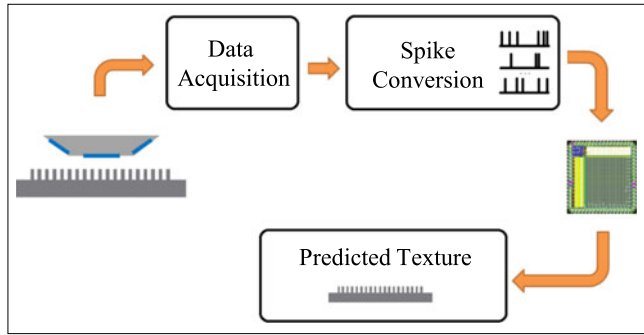


Fig. 1. An illustration of the neuromorphic system for texture recognition. The textured surface is touched at a uniform pressure and speed using an artificial finger equipped with an array of tactile sensors. Output of the tactile sensor is converted into spike patterns then transmitted to a neuromorphic ELM chip for processing.

and scalable solutions. We had previously demonstrated object recognition capability of the proposed system in our preliminary work which was presented at the IEEE Biomedical Circuits and Systems Conference [22].

Our platform consists of a piezoresistive fabric material as the sensor to emulate skin, an interface that produces spike patterns to mimic neural signals from mechanoreceptors [4] and an ELM chip [45] to analyze spiking activity. The ELM architecture was selected for processing of tactile data because of its fast training speed [46] and ease of hardware implementation [47]. A fast and simple training strategy is of significant importance for our application since sensor properties drift over time and require quick recalibration. Ease of hardware implementation is also a desired feature for robotic and embedded applications. An illustration of this framework is provided in Fig. 1.

The rest of this paper is organized as follows. Section II provides an overview of the system, including sensor design, neuronal models, decoding algorithm, and the ELM chip. Section III describes the experimental design. Section IV provides a summary of our results and major findings. Section V presents the discussion and concluding remarks.

II. MATERIALS AND METHODS

A. The Artificial Touch Sensor

A biomimetic tactile sensor array was fabricated to sense shear and normal forces. The sensor array comprised of ridge-shaped structures with force sensitive components on each side. A transparent acrylic foam adhesive (VHB 4910 acrylic tape, 3M, USA) was used to construct the substrate and ridge structures. Force sensitive elements were built by sandwiching a piezoresistive material (Stretchy Piezo LTT-SLPA-150k, Eeonyx, USA) between two conductive layers (Silver plated mesh, LessEMF, USA). When pressure is applied at these sensing elements, the resistance of the piezoresistive material alters which can be detected by measuring the impedance between top and bottom electrodes. The characteristic relationship between the applied force and resistance of the piezoresistive material is provided in [48]. However, in this work, we are not concerned about the exact value of applied forces. The sensor array (2×3

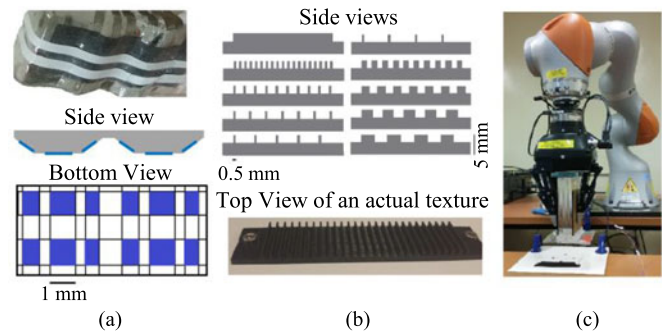


Fig. 2. Experimental setup for texture recognition. (a) Architecture of the fabric based tactile sensor. Sensing is achieved using a piezoresistive material sandwiched between two conductive layers. Each blue rectangle in the lower panel identifies a sensing element, located at crossover of top and bottom electrodes. (b) 3D-printed graded textures, and (c) Kuka robot and the Barret hand gripper holding the artificial tactile sensor mounted on a rectangular cubic object.

taxels) consisted of two ridge structures that were separated from each other with a distance of 1 mm and conductive electrodes measured 1 mm in width. The structure of the sensor is illustrated in Fig. 2(a).

B. Robotic Platform

To standardize this procedure and control tactile stimuli precisely, the experiments were performed using an industrial robotic arm and ten graded textures. A detailed descriptions of the robotic setup, textured surfaces and experimental procedures are provided below.

1) *Robotic Setup*: The experiments were performed using a Kuka LBR iiwa Robot (KUKA Robotics Corporation, Germany) that was equipped with a Barrett Hand Gripper (Barrett Technology LLC, USA) as the end effector. The tactile sensor array was mounted on the bottom of an artificial fingertip (a rigid rectangular bar with dimensions $5 \text{ cm} \times 5 \text{ cm} \times 20 \text{ cm}$) gripped by the Barrett Hand. Textures were mounted on a static platform while the Kuka robotic arm was used to indent and slide the fingertip over the textures. The robotic setup is depicted in Fig. 2(c). The robot was operated in a 2 degree of freedom (DoF) trajectory. Force control was used in the z direction to control the pressure exerted on the textured surface. Velocity control was used in x direction to control the speed of sliding along the texture.

2) *Textures*: Ten graded textures were fabricated using 3D printing (see Fig. 2(b)). A minimum ridge width of 0.5 mm was selected for fabrication of 3D textures to achieve thin yet durable ridges. Wider ridges, particularly those larger than the e-skin resolution, excite multiple taxels upon contact. Smaller ridges have higher probability of failure and damage during the experiment. A minimum pitch of 0.5 mm was used to assess the recognition capability of our system. Ridge width and pitch were varied to recreate different textures. An illustration of these textures is provided in Fig. 2(b).

3) *Experimental Protocol*: To obtain sensor outputs for fabricated textures, we used a passive touch protocol. Each texture was fixed on a static platform, while the fingertip was slid over

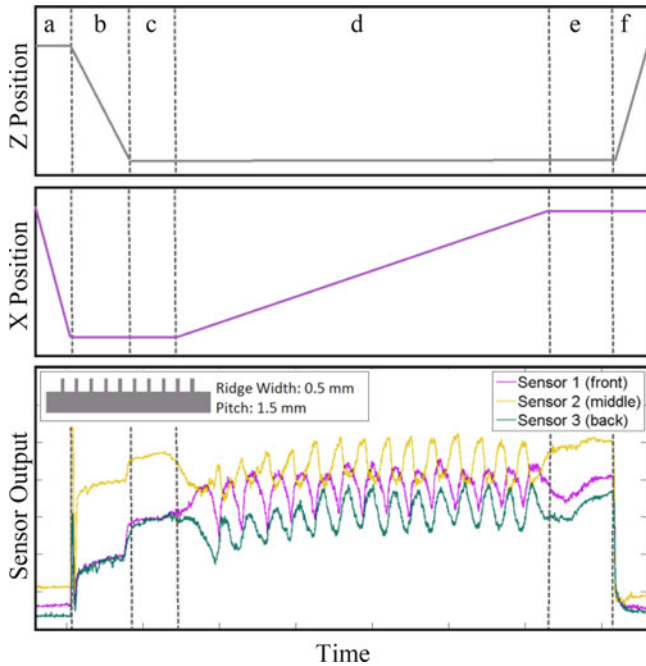


Fig. 3. Kuka robot movement profile (top and middle panels) and typical sensor outputs (bottom panel). The experiment consists of six steps. (a) Preparation phase: the robot goes to a predetermined position. (b) Indentation phase: the artificial finger is pressed against the textured surface. (c) Rest phase: stabilizes the initial conditions. (d) Sliding phase: artificial finger slides in the x direction, which is along the textured pattern. (e) Rest phase: stabilizes the condition. (f) Lift phase: artificial finger is moved away from the texture. Force control was used in the z direction to precisely control pressure magnitude exerted over the textured surface. Velocity control was used in x direction to manage the speed across the texture.

the texture by the Kuka robotic arm. The fingertip was initially placed 50 mm above the texture (preparation phase). Next, it was moved down (z -axis) until contact was made with the textured surface and reached a desired contact force (indentation phase). After one second, the fingertip was slid over the texture (x -axis) for a distance of 50 mm with a fixed sliding velocity of 5 mm/s. Upon completion of movement over the textured surface, the fingertip was held still for 1 s in contact mode (indentation after sliding phase). Lastly, the robotic arm with sensorized finger was retracted to the initial position (retraction phase). This procedure was repeated three times for each texture. An illustration of this approach and typical sensor outputs are shown in Fig. 3.

C. Data Acquisition

To acquire outputs at each taxel, the sensor array was scanned in a sequential manner [26]. The data acquisition circuit is illustrated in Fig. 4. During each step, one row was excited with a logical high while other rows were set to a logical low. A potential divider circuit was used to obtain voltage readouts corresponding to the resistance at particular cross sections of the array. The measured values were converted to digital values using an analog-to-digital converter (ADC). The array was scanned at 300 Hz. The readout circuit was controlled using a NXP LPC1768 Microcontroller.

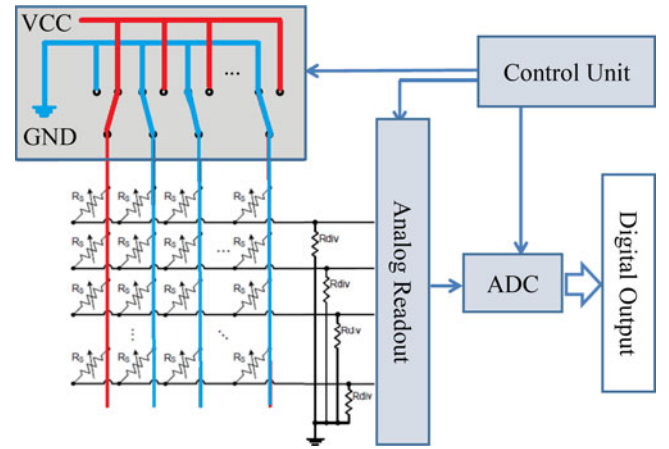


Fig. 4. Sensor readout circuitry. To acquire outputs at each taxel, the sensor array was scanned in a sequential manner.

D. Neuronal Model

We emulate the behavior of mechanoreceptors in the skin for conversion of tactile information into digital spikes. Mechanoreceptors innervating the glabrous human skin are categorized into two major categories (1) slow adapting (SA) and (2) fast adapting (FA) [4]. SA receptors produce spikes at a frequency proportional to intensity of stimulus, while FA receptors respond to changes of stimulus intensity [49]. SA receptors provide encoding of pressure and FA receptors encode transient behavior of the signal. These receptors are further categorized as Type 1 and 2. Type 1 receptors typically have a smaller receptive field and are located close to the surface of the skin, while Type 2 receptors have larger receptive fields and are located deeper in the skin [49].

We implemented three types of receptors: (1) SA receptors that produce spikes with a frequency proportional to the sensor output, (2) FA-Rising receptors that respond to an increase in amplitude of a dynamic stimulus, and (3) FA-Falling receptors that encode a decrease in amplitude of a dynamic stimulus. Although this implementation has been inspired by physiology of FA and SA mechanoreceptors, it differs significantly from its biological counterpart. Human FA mechanoreceptors respond to both decrease and increase of a dynamic stimuli, while our model includes two separate receptors for encoding positive and negative changes to increase information content of spike trains. Here, our goal is not to strictly model human mechanoreceptor. We are primarily concerned with developing a texture recognition system by selectively mimicking the desirable dynamic properties of the human skin. A comparison of responses from two typical human SA-1 and FA-1 mechanoreceptors and responses of our simulated receptors are provided in Fig. 5.

To mimic the spiking activity produced by a receptor in the skin, we use a model to convert the analog (touch) to digital (spikes). In our implementation, an Izhikevich neuronal model [50] is used to convert tactile signals into spikes. An illustration of this model and relevant parameters is provided in Fig. 6. We select the Izhikevich model because it is capable of reproducing a large range of neuron dynamics. In an Izhikevich neuron model, the membrane potential of the neuron v and an adaptation

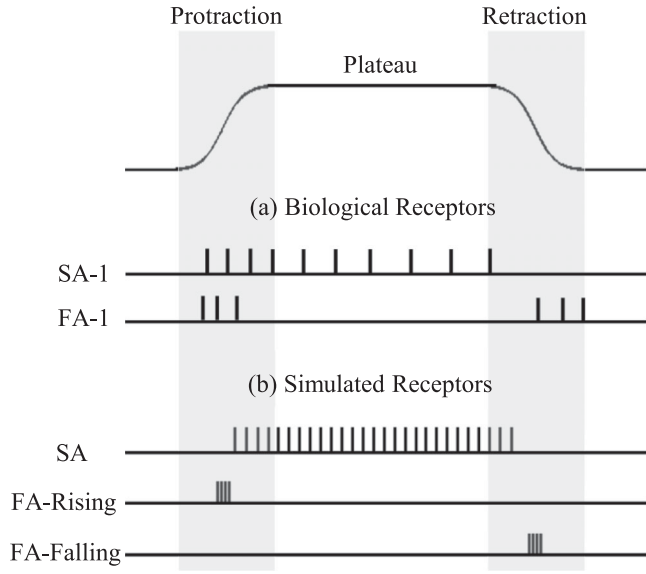


Fig. 5. An illustration of responses of (a) actual human SA-1 and FA-1 receptors (adapted from [4]), and (b) simulated SA, FA-Rising, and FA-Falling receptors. SA receptors provide a measure of the signal amplitude, and FA receptors encode transient behavior of the signal. While human FA mechanoreceptors respond to any transient events (including both decrease and increase of a dynamic stimuli), our model includes two separate receptors for encoding positive and negative changes in the signal amplitude.

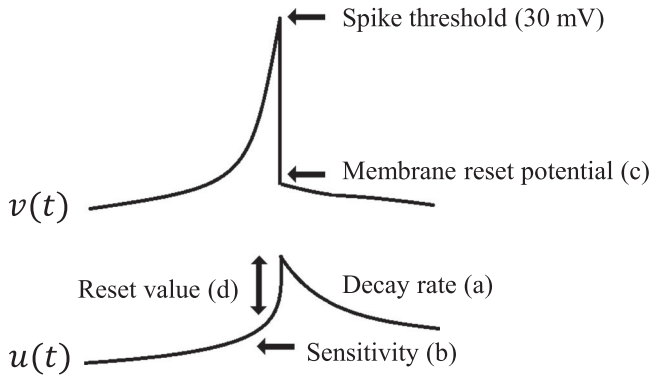


Fig. 6. An illustration of Izhikevich neuron model and relevant parameters. The membrane potential of the neuron (v) and the adaptation variable (u) are updated using Euler's method as described by 1. The parameters a , b , c , and d are chosen to produce a desired spiking behavior. The parameter a determines decay rate, b controls sensitivity to spikes, c regulates membrane reset voltage and d governs reset value of the adaptation variable.

variable u are updated using Euler's method as

$$\dot{v} = Av^2 + Bv + C - u + \frac{I_{\text{input}}}{D}, \quad (1)$$

$$\dot{u} = a(bv - u), \quad (2)$$

$$\text{if } v \geq 30 \text{ mV, then } \begin{cases} v \leftarrow c \\ u \leftarrow u + d \end{cases} \quad (3)$$

where I_{input} is the neuron's input current, and A , B , C , D are standard parameters of the Izhikevich neuron model which are set to 0.04, 5, 140, and 1, respectively. Parameters a , b , c , d are chosen to produce a desired spiking behavior. The parameter

TABLE II
PARAMETERS OF THE IZHIKEVICH NEURON MODEL

Receptor Type	Firing Behavior	a	b	c	d
SA	Regular Spiking (RS)	0.02	0.2	-0.65	8
FA-Rising	Fast Spiking (FS)	0.1	0.2	-0.65	2
FA-Falling	Fast Spiking (FS)	0.1	0.2	-0.65	2

a determines the decay rate, b controls sensitivity to spikes, c regulates membrane reset voltage, and d governs reset value of the adaptation variable. When the membrane potential reaches a spike threshold (typically 30 mV), a single spike is produced and the membrane potential is reset.

The parameter values that are used in this study are listed in Table II. These values are selected to emulate the Regular Spiking (RS) and Fast Spiking (FS) firing patterns [51] for SA and FA (FA-Rising and FA-Falling) receptors, respectively. An RS-type neuron, when injected with a supra-threshold current, initially fires at a relatively high rate but rapidly slows its firing rate and reaches a constant-frequency firing rate (determined by the amount of injected current) [51]. This characteristic helps encode amplitude of the stimuli, and thus, is suited to model signaling behavior of SA receptors. A FS-type neuron shows less adaptation and can fire at a significantly faster rate than a RS-type neuron. This characteristic is desirable for modeling FA receptors, and is achieved by a selecting a low value for parameter d (lower adaptation) and a higher value for parameter a (faster decay) [51], [52].

To convert sensor outputs into spikes, sensor values were first normalized (divided by the maximum possible sensor value) and were converted into three signal types: (1) SA, which is the normalized sensor output, (2) FA-Rising, which is positive values of the derivative of the normalized signal, and (3) FA-Falling, which is absolute of negative values of the derivative of the normalized signal. These signals were then multiplied by a gain factor (GF) and used as the input current (I_{input}) of the Izhikevich neuron model. This can be expressed as

$$I_{\text{SA}} = GF \times V_{\text{Sensor}}$$

$$I_{\text{FA-Rising}} = GF \times [dV_{\text{Sensor}}/dt]^+$$

$$I_{\text{FA-Falling}} = GF \times |[dV_{\text{Sensor}}/dt]^-| \quad (4)$$

where V_{Sensor} is the normalized sensor output, I_{SA} , $I_{\text{FA-Rising}}$, and $I_{\text{FA-Falling}}$ are currents of SA, FA-Rising, and FA-Falling neurons, $| \cdot |$ denotes the absolute value, and $[\cdot]^+$ and $[\cdot]^-$ identify positive and negative values of a signal, respectively. Fig. 7 illustrates a typical sensor output and spikes produced for one experimental texture. The top panel shows the normalized sensor output, second and third panels depict SA and FA currents, and the last three panels illustrate generated spikes.

To identify an appropriate value for GF, we measured the inter-spike interval (ISI) distribution of receptors for a large range of GFs. The results are presented in Fig. 8, where a fitted distribution for every texture is plotted for clarity.

The plots show that increasing the GF results in a monotonic decrease in the ISI (indicating an increase in firing rate) as well

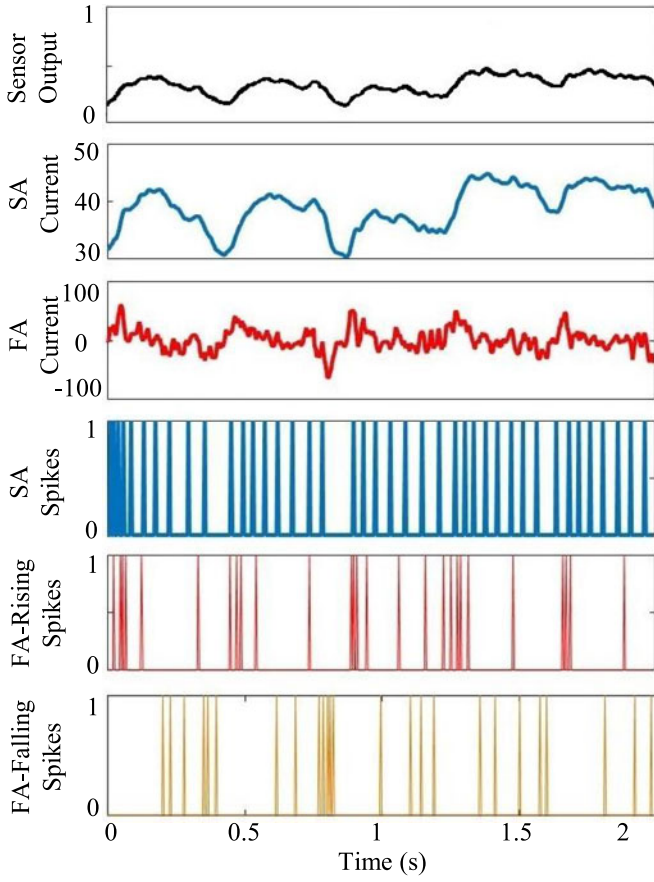


Fig. 7. Typical sensor outputs and generated spikes for one of experimental textures (ridge width: 1 mm, pitch: 1 mm). An Izhikevich neuron model is used for conversion of tactile signals into spikes. SA spikes are generated by using the normalized sensor outputs. FA-Falling spikes are generated by using positive and absolute of negative values of the derivative of normalized sensor outputs, respectively. These values are first multiplied by a GF, and then are converted into spikes using the Izhikevich neuron model.

as an increase in overlap of ISI distributions of different textures (indicating lower diversity among spike patterns). In contrast, lower firing rates lead to encoding problems for two reasons. (1) A reduced set of responses on short timescales and (2) a longer latency of responses affecting real-time applications. Therefore, we select an intermediate value of GF for all receptors. The maximum input spike rate that the ELM chip can process using our experimental setup is 640 Hz. For this reason, we selected $GF = 50/\Omega$ for SA receptors and $GF = 5000/\Omega$ for FA-Rising and FA-Falling receptors. This results in an average spike rate of approximately 100 Hz, which is a range similar to that of human SA mechanoreceptors [53].

E. The Neuromorphic Classifier

1) *ELM Algorithm*: An ELM is a single hidden layer feed-forward neural network (SLFN) where the input weights are randomized [54]. The output of the ELM is expressed as

$$y_k = \sum_{i=1}^L \beta_{ik} h_i = \sum_{i=1}^L \beta_{ik} g(\mathbf{w}_i^T \mathbf{x} + b_i) \quad (5)$$

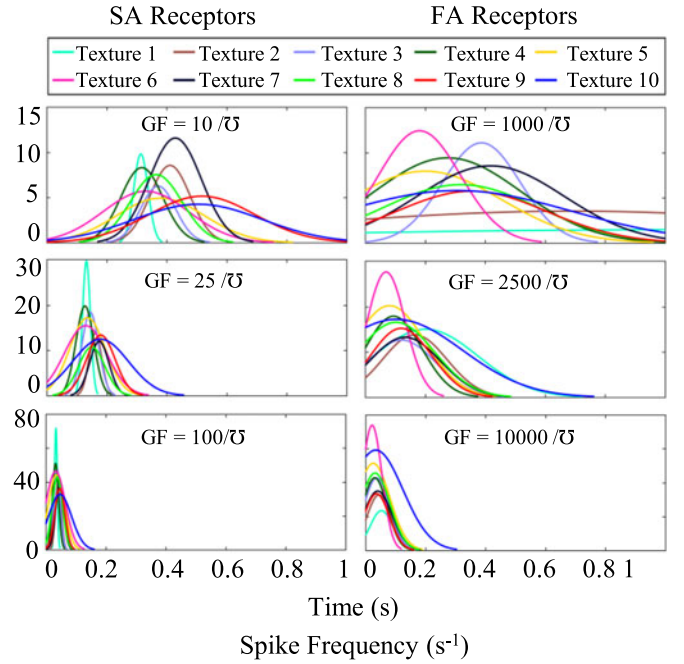


Fig. 8. ISI histograms of textures for different current gain factors. A fitted distribution for histograms of every texture is plotted for clarity. Histogram of SA receptors are plotted on the left side, and histogram of FA-Rising receptors are plotted on the right side.

where y_k denotes the k -th output of the network ($1 \leq k \leq C$, where C is the number of classes), L is the number of hidden layer nodes, h_i is the value of the i -th hidden layer neuron, β_{ik} is the weight between the i -th hidden layer neuron and the k -th output, \mathbf{x} is the input vector, $\mathbf{w}_i = [w_{1i}, w_{2i}, \dots, w_{mi}]^T$ are the weights between the input layer and hidden layer node i , and b_i is the bias of hidden layer neuron i . A non-linear activation function $g()$ is typically used for regression and classification. In contrast to traditional training approaches where all weights are tuned by backpropagation, input weights and biases \mathbf{w}_i and b_i for $i = 1, \dots, L$ are randomly selected and fixed after the random initiation. Thus, only output weights need to be tuned in ELM.

Equation (5) can be written in matrix form as

$$\mathbf{H}\beta = \mathbf{Y} \quad (6)$$

where \mathbf{H} is the hidden layer output matrix of the neural network, β is matrix of network output weights, and \mathbf{Y} represents the network output matrix for N input data.

During the training phase, output weights are obtained by solving the least-squares solution to

$$\mathbf{H}\beta = \mathbf{T}, \quad (7)$$

where \mathbf{H} is the hidden layer output matrix and $\mathbf{T} = [T_1, \dots, T_N]$ is the target of the training data. The output weights are derived analytically as

$$\beta = \mathbf{H}^\dagger \mathbf{T}, \quad (8)$$

where \mathbf{H}^\dagger denotes the Moore-Penrose generalized inverse of the hidden layer output matrix.

During the decoding phase, outputs of hidden layer nodes are obtained and used to calculate the response of the output neurons using 6. The final classification decision is achieved by selecting the output neuron with the highest activation value

$$s^j = \arg \max_k y_k^j, \quad 1 \leq k \leq C \quad (9)$$

where C is the number of classes, y_k^j is the value of the k th output node for input sample j , and s^j identifies the predicted class label for input sample j .

2) *Time-Delayed ELM*: The ELM, in general, is not capable of processing time coded and dynamic signals. It produces an output based on input features at every moment. Similarly, the customized ELM chip is only capable of decoding rate coded signals as it measures the average number of input spikes in every channel during a counting time window. This limits its application for analysis of time-coded and dynamic signals. The common approach to mitigate this problem is to extract and use features that represent dynamic behavior of the signal. However, this approach demands for a specialized feature extraction step which makes it application-specific. Here, we use an algorithmic approach proposed by [45] to overcome this limitation. The proposed method is based on the use of time-delayed input signals as features. We construct a new input pattern using time-delayed input signals. If $n_d - 1$ delayed version of the input signals are used, the new input pattern can be represented as

$$\mathbf{x}(t_k) = [\mathbf{x}(t_k), \mathbf{x}(t_k - 1), \dots, \mathbf{x}(t_k - n_d + 1)], \quad (10)$$

where $\mathbf{x}(t_k)$ is the original input data at time t_k and $\mathbf{x}(t_k - i)$ is the i th delayed version of the signal. The input dimension of the new input pattern is given by $D = n_d \times m$, where m is the dimension of original input data.

3) *ELM Processor*: We use a customized ELM chip [55] to project the input data into a higher dimensional space to produce the hidden layer outputs. The ELM chip has 128 input channels and 128 hidden layer nodes. Each input channel embeds a processing circuit that extracts features from a spike train. A window counter in the input processing circuit records the number of spikes in a moving time window. The counter value is converted into an input feature current by a current DAC which is further mirrored into 128 hidden layer nodes by a current mirror array. The ratios of the current mirrors are the input weights. Although identical transistors are used to design the current mirror array, these weights are random due to fabrication mismatches. High computational efficiency is achieved by exploiting the random mismatch and massively parallel analog computing. In this work, the second layer computations are done on a PC. However, they can be easily transferred to a microprocessor or a custom IC [56].

F. Classification Metrics

We characterize classification performance of our system using two important metrics: classification accuracy, and information measure. A brief description of these measures are provided in the following.

1) *Classification Accuracy*: Classification accuracy is one of the most widely used metrics for evaluating the performance of a classifier. It evaluates the effectiveness of the classifier by its percentage of correct predictions. Classification accuracy is calculated by dividing the numbers of correctly predicted labels by the total number of samples.

2) *Information Transfer Rate*: Information theory is widely used in neural systems to understand the statistical details embedded in spike trains [57]. The information encoded in neural recordings are measured by the ability to discriminate various stimuli based on their spike train response. This metric presents a more objective performance measure compared to classification accuracy since it provides information about the error distribution [58]. We use Shannon's information measure [59] to compute the mutual information between the ground truth label (L) and classifier response (R) which is expressed as

$$I(R; L) = \sum_{R, L} p(R|L) \cdot p(L) \log_2 \frac{p(R|L)}{p(R)} \quad (11)$$

where $p(R|L)$ is the probability of classifier predicting response R for an input L . These probability values can be obtained from the confusion matrix.

III. EXPERIMENTS

Efficiency of a hardware-based classifier depends on several factors, most importantly recognition accuracy, response time, and energy consumption. In this section, we provide an overview of our designed experiments to characterize some of these parameters, namely the classification accuracy, decision time, and time-to-recognition. Moreover, we discuss the effect of input spike rate on classification accuracy and energy consumption. Detailed description of each experiment is provided in the following.

A. Texture Decoding

Textures are decoded by classifying corresponding spike patterns over the sampling time window. We use n_d delay channels for every input channel. This allows us to process spatiotemporal patterns and to cover a larger sampling window of length $T_s = n_d \times T_w$ using a counting window of length T_w . In this experiment, we use a sampling window of 1 s, which is the time required by the artificial finger to slide over the largest spacial period among all textures. Each sample is divided into $n_d = 10$ time windows of equal length $T_w = 100$ ms to be used as input features for the ELM classifier. This results in a total number of 90 features as inputs for the ELM chip (3 sensors \times 3 receptor types \times 10 signal intervals).

Sensor values for a period of 5 s for each texture are collected. Measured signals are then divided into 50 data samples of length 1 s for each texture by sliding a sampling window of 1 s at 100 ms time intervals. The purpose is to create samples with various starting points along the textured surface for robust and location-independent performance. During the training phase, 60% of the 50 generated samples for each texture are selected randomly

and used to train the system, while 20% of samples are used as the validation dataset to optimize parameters of the learning algorithm (output weights, and the regularization factor). The system is then tested against the remaining 20% of samples.

B. Decision-Time Analysis

The ELM chip counts the number of spikes in every channel over a counting time window and produces an output at the end of this period accordingly. Thus, a decision can only be made after this time period ends. A faster decision can be made by using a smaller time window. However, a shorter time window is associated with a smaller sampling time and thus may deteriorate the classification performance. We investigate this trade-off through analysis of the classification accuracy and information transfer rate for various counting time windows.

C. Time-to-Recognition Analysis

Early detection and characterization is an appealing feature for many applications. While decision time analysis is concerned with finding the effect of counting and sampling time windows on classification performance, the time-to-recognition analysis investigates the propagation of information in the system over time. To get the classification outcome, the system needs to wait till reliable information is propagated in each of the channels. We evaluate time-to-recognition characteristics of our platform by analyzing the classification accuracy at every time step from beginning of the sliding motion.

D. Spike-Rate Analysis

Input spike rate has significant effects on the classification accuracy and the power consumption. While low spike rates offer lower energy consumption, they may lead to encoding problems due to limited response diversity and latency issues. On the other hand, higher spike rates generally offer better encoding possibilities, but suffer from higher energy consumptions. It should be also pointed out that extremely high spike rates may lead to a decrease in response diversity, and thus lower classification accuracy, due to neuron's adaptation and refractory characteristics and limited time resolution. We investigate the effect of input spike rate on classification accuracy and energy consumption by varying the input spike rate. Spike rate is altered by adjusting the GF of the Izhikevich neuron. Higher rates are achieved by increasing the GF.

IV. RESULTS

This section presents our findings about decoding performance of our system and effect of various parameters on classification accuracy. The characterization results for decision time and time-to-recognition analysis are provided, and the effects of input spike rate on classification accuracy and energy consumption are discussed.

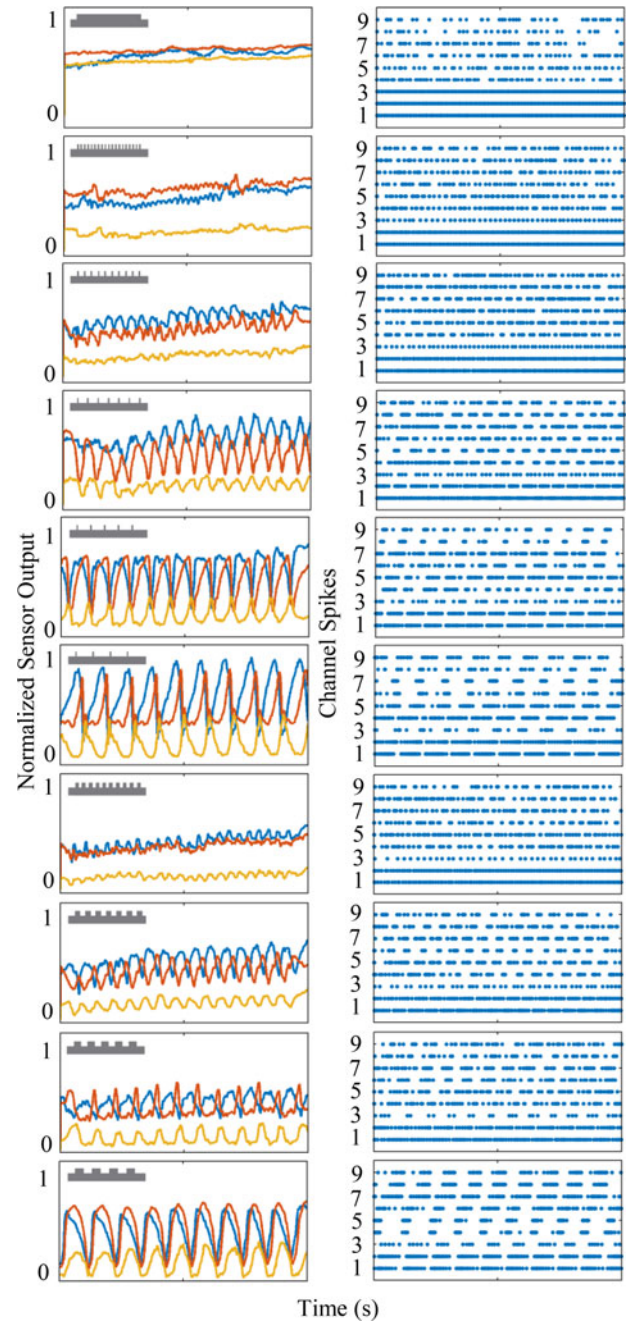


Fig. 9. Sensors outputs and associated spike rasters for ten graded textures. Each row represents the data for one textured surface. The texture is depicted in top left corner of the left plot. The plots on the left illustrate normalized sensors outputs (front, middle, and back sensors) obtained by sliding the artificial fingertip on the textured surface, and the plots on the right illustrate generated spike patterns. Each dot represents a spike. Channels 1-3 model the response of SA receptors, while channels 4-6 and 7-9 represent the responses of FA-Rising and FA-Falling receptors, respectively. The generated spike pattern from each texture acts as a signature that can be used to identify that texture.

A. Texture Decoding

Every texture is associated with a spatiotemporal spike pattern in which the spatial dimension determines location of sensors and the temporal dimension identifies development of sensor outputs (spikes) over time. An illustration of spike patterns for fabricated textures is provided in Fig. 9.

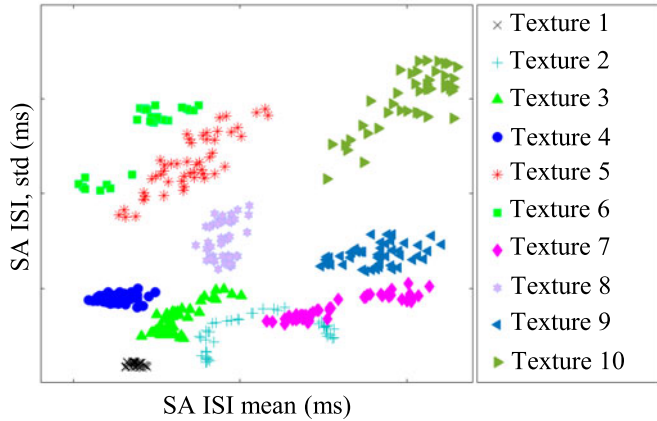


Fig. 10. Spike train statistics. Each point on the plot determines ISI statistics for a 1 s data sample from a texture. Fifty data samples from each texture are plotted. The x-axis identifies the mean value of ISI of SA receptors, and y-axis identifies its standard deviation.

Texture classification can be simply translated to decoding corresponding spike patterns. Evidently, a good classification performance demands for distinguishable spike patterns. To investigate distinguishability of elicited spike patterns, we calculated their ISI statistics. Fig. 10 plots ISI mean value and its standard deviation for SA and combined FA receptors (FA-Rising and FA-Falling). As it is illustrated, spike timing statistics can be used to distinguish the textures. This is consistent with results reported by [8]. They showed that spike statistics and spike train distances can be used for texture categorization.

To evaluate texture classification capability of our system, we presented spike patterns of the test samples to the trained ELM classifier. A counting window of 100 ms and 10 input channels per sensor output (9 delayed channels per sensor, each implementing a delay of 100 ms) were used for this experiment. Classification outcome for every sample was determined at the end of the first second. Fig. 11 presents the average classification accuracy and confusion matrix for this experiment. As it is illustrated, the system is capable of predicting the correct class label with an accuracy of 92%. It performs well in recognizing all textures, except texture 5 which gets confused with textures 4 and 6.

B. Decision Time Analysis

A classification decision can only be made after a counting time window is complete. We investigate the effect of this waiting time on classification accuracy and information transfer rate. These results are presented in Fig. 12.

As it is illustrated, there exists a trade-off between decision time and accuracy. A longer decision time results in a higher classification accuracy at the expense of a longer response time. This is because more information becomes available about the stimuli by observing its behavior over longer sampling periods (Fig. 12). While a longer response time might be acceptable in some applications, it may not satisfy the requirements of real-time applications. Therefore, the value of this parameter and its

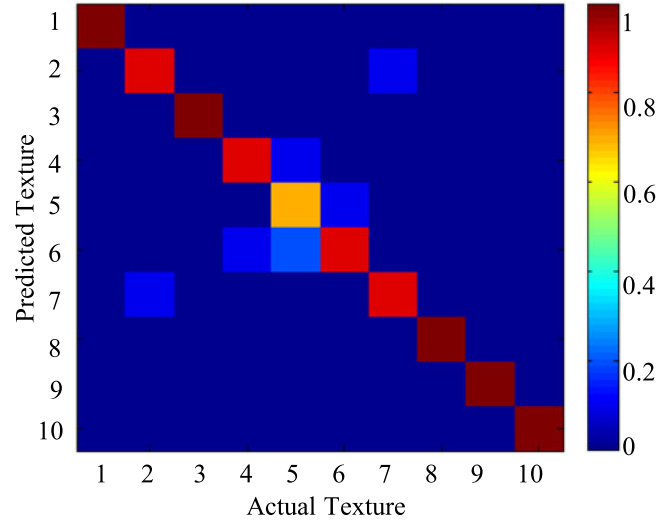


Fig. 11. Confusion matrix for texture classification. Nine delayed channels per sensor output were used for the experiment, each having a counting window of length 100 ms and a delay of 100 ms compared to its preceding channel.

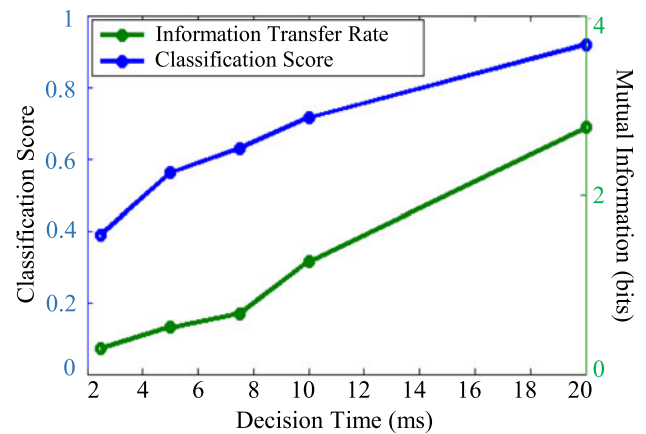


Fig. 12. Effect of decision time on classification accuracy and information transfer rate. Decision time is defined as the time required to reach a classification decision. This is equivalent to the length of the counting time window T_w in our experimental setup. Nine delayed channels per sensor output were used for the experiment, each having a counting window of length T_w and a delay of T_w compared to its preceding channel.

effect on classification performance should be well considered while designing a real-time system.

C. Time-to-Recognition Analysis

The results presented so far were obtained using samples that covered a full sampling period. This setting, however, is not valid at early time steps. For example, when the fingertip starts its sliding motion over the textured surface or shifts to another one, the newly generated spikes are not propagated across the channels. Thus, a classification decision is prone to error. We characterized this effect with the goal of finding the earliest time that the classification outcome becomes valid.

Towards this goal, we first investigate the similarity of texture spike patterns at different time steps. This is done by calculating

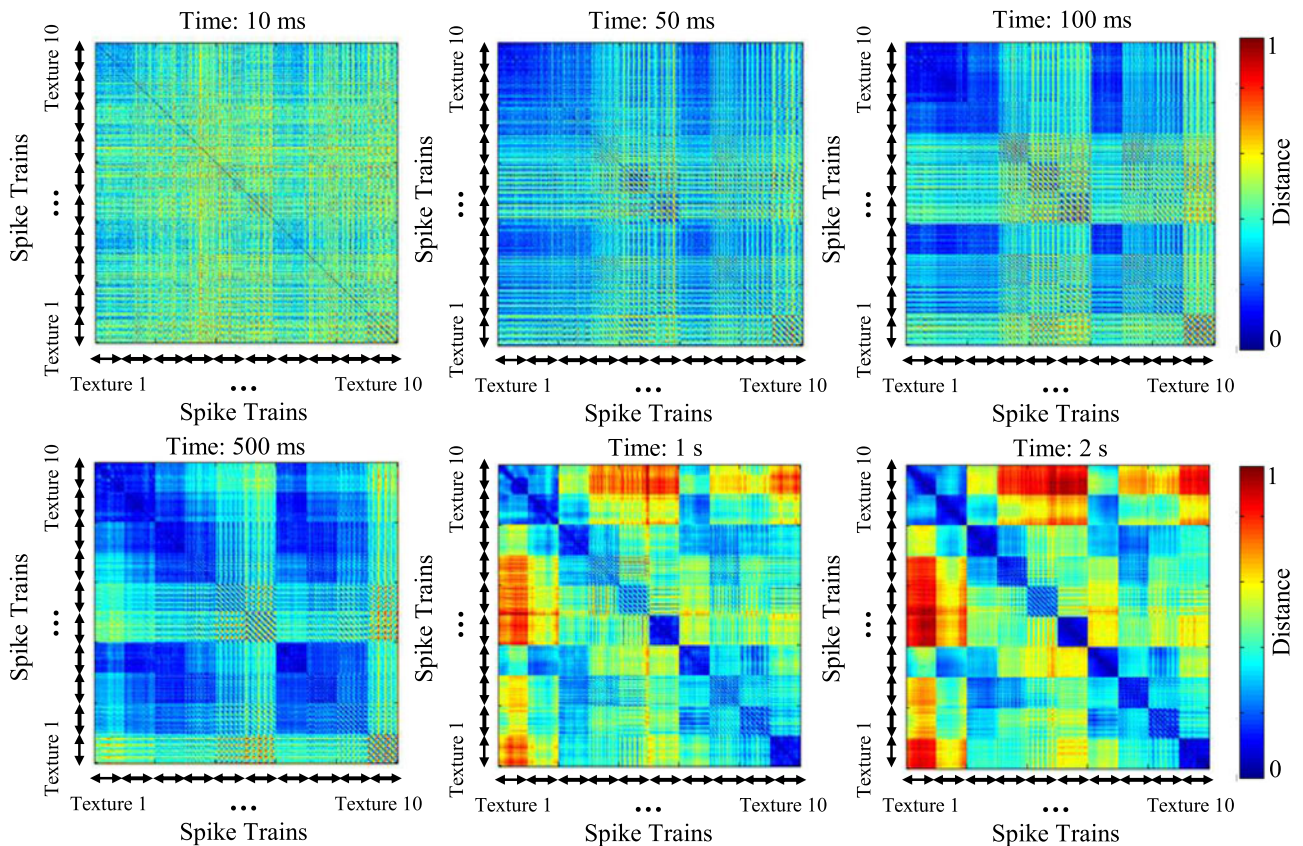


Fig. 13. Euclidean distances between spike trains. Spike trains were generated by sliding the artificial finger over the textured surfaces. The inter-class distances increase as time passes, while intra-class distances decrease.

a distance measure between spike patterns. Larger distances indicate lower similarity between the patterns. We use a Euclidean distance measure calculated on binned spike patterns instead of a direct spike-based distance metric. That is because the ELM classifier receives and categorizes the binned spike patterns. Fig. 13 presents calculated distances between spike patterns at several time steps after commencing the sliding motion. As it is illustrated, all spike patterns have similar distances at the beginning of the movement. As time passes, distances between similar patterns decrease, while distances between different patterns increase, and thus patterns become more distinguishable.

We further characterized classification accuracy of the system at various time steps. Results are presented in Fig. 14. As it is illustrated, classification accuracy is extremely low at initial time steps and increases monotonically with time. This is consistent with results obtained by analysis of Euclidean distances of binned spike trains.

D. Spike Rate Analysis

Fig. 15 illustrates the effect of spike rate on classification accuracy, transferred information, and energy consumption of the ELM chip. Spike rate was varied by adjusting the GF of the Izhikevich neuron. As it is illustrated, accuracy drops slowly at first when spike rates are reduced till about a rate of 10 Hz. For rates lower than this, the drop in accuracy is significant. This is mainly due to loss of information in low spike rates

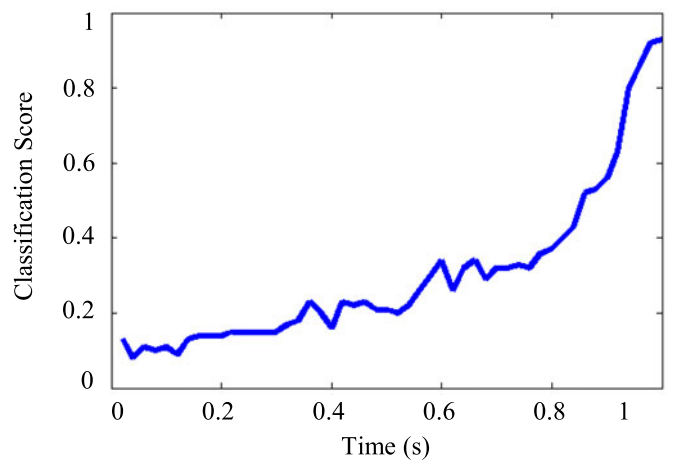


Fig. 14. Classification accuracy over the time. Performance of the system was measured over time to find the minimum time required for reliable decoding of textures. Classification accuracy reaches its maximum value at about 1 s.

where spike trains become indistinguishable. Higher spike rate, however, translate in higher energy consumption. Thus, a trade-off arises for selecting the appropriate spike rate. To address this trade-off, we consider the accuracy-energy consumption plot (Fig. 16). This plot helps select the pareto-optimal spike rates by identifying the pareto-optimal front.

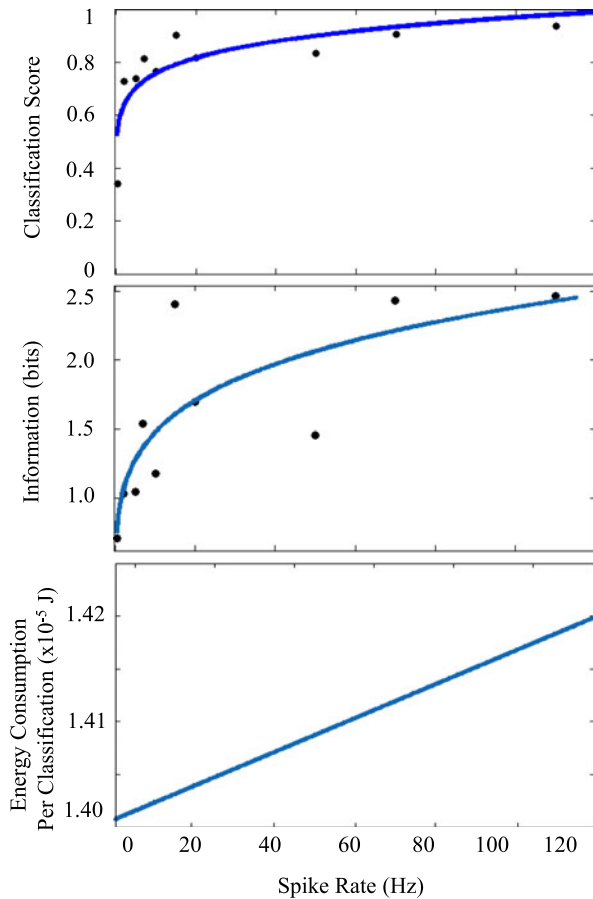


Fig. 15. Effect of spike rate on classification accuracy and transferred information. Spike rate is controlled by adjusting the current gain of the Izhikevich neuron.

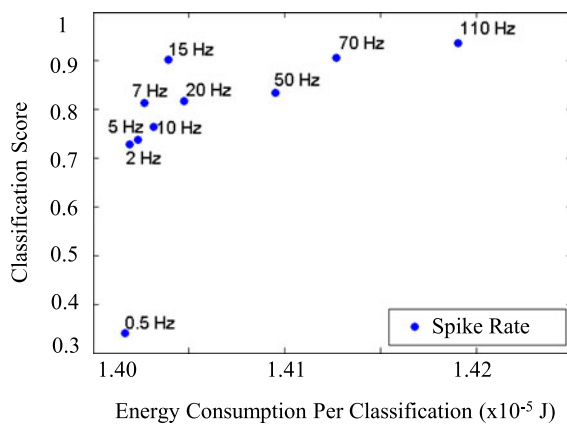


Fig. 16. Top: Effect of spike rate on classification accuracy. Bottom: classification score versus energy consumption per classification. A pareto-optimal point from the pareto set can be selected to balance the accuracy-energy consumption trade-off.

V. DISCUSSION AND CONCLUSION

We presented a neuromorphic system for tactile-based texture recognition. Our system comprised a fabric-based piezoresistive force sensor that emulated the skin, an interface for producing spike patterns that emulated the neural signals from the mechanoreceptors in the skin, and an ELM chip for computing

and pattern recognition. We demonstrated recognition capability of our system in a texture recognition task where it achieved a classification accuracy of 92% for categorization of 10 graded textures. Our results confirmed that an integrated hardware-based neuromorphic system for tactile texture recognition is achievable.

We demonstrated that there exist a trade-off between decision-time and classification accuracy (and information transfer rate). A faster decision time was achieved by using a shorter time window. This, however, resulted in deterioration of classification accuracy and information transfer rate. A similar trade-off was observed between classification accuracy and time-to-recognition. Classification accuracy was extremely low at early time steps due to similarity of all spike-patterns. Classification accuracy and information transfer rate increased at longer time periods as more information became available and spike patterns became more distinguishable. These response time characteristics are particularly important for time-critical applications and active perception. In these scenarios, early detection of desired patterns are of significant importance. For example, in active palpation, information obtained at initial time steps, even if not complete and accurate, can be used to execute an appropriate action at early time steps to increase the information gain and efficiency.

We further characterized energy consumption of the developed system as it is another important characteristic that determines efficiency and usability of a hardware-based system for real-life applications. Our results confirmed that although the system consumes minimal energy at low spike rates, it suffers from low classification accuracy and information transfer rate. Higher spike rates resulted in higher classification accuracy and information transfer rate. However, this relationship may not be monotonically-increasing as spike patterns may become indistinguishable at extremely high spike rates. However, we did not observe such effect in our experiments as our maximum spike rate was constrained due to limitations of the ELM chip.

Although capability of the developed neuromorphic system for tactile pattern recognition was demonstrated, it is far from a complete solution. It only presents integration of sensors with neuromorphic implementation of one of many available machine learning algorithms. ELM was selected due to its general applicability and ease of hardware implementation. However, it has several disadvantages, including inherent incapability of processing temporal patterns and lack of robustness due to randomness of network weights. An important extension of this work may involve neuromorphic implementation of learning algorithms that are capable of real-time processing of spatio-temporal spike patterns. Although our system is capable of processing spatio-temporal spike patterns, it achieves so by constructing spatio-temporal features from time-delayed data. A neuromorphic algorithm that can overcome this limitation is highly desirable.

Present study aimed to explore the opportunity for development of compact neuromorphic systems that are capable of processing spike-based sensory information. Such systems can help achieve energy-efficient solutions for processing of sensory information by exploiting inherent advantages of event-based architectures. Moreover, such tactile modules are capable of

local-processing of information and extraction of high level features. This helps utilize the communication bandwidth and other resources more efficiently by eliminating the need for transfer of redundant data and interrupting other resources. These features can pave the way for development of low-cost modules for large-area coverage which has significant implications for robotic and prosthetic applications.

REFERENCES

- [1] A. Chortos and Z. Bao, "Skin-inspired electronic devices," *Mater. Today*, vol. 17, no. 7, pp. 321–331, 2014.
- [2] A. Chortos, J. Liu, and Z. Bao, "Pursuing prosthetic electronic skin," *Nature Mater.*, vol. 15, pp. 937–950, 2016.
- [3] R. S. Dahiya and M. Valle, *Robotic Tactile Sensing: Technologies and System*. New York, NY, USA: Springer, 2012.
- [4] R. S. Johansson and J. R. Flanagan, "Coding and use of tactile signals from the fingertips in object manipulation tasks," *Nature Rev. Neurosci.*, vol. 10, no. 5, pp. 345–359, 2009.
- [5] S. J. Lederman, *The Perception of Texture by Touch*, W. S. E. Foulke, Ed., Cambridge, U.K.: Cambridge Univ. Press, 1982.
- [6] K. E. Friedl, A. R. Voelker, A. Peer, and C. Eliasmith, "Human-inspired neurorobotic system for classifying surface textures by touch," *IEEE Robot. Autom. Lett.*, vol. 1, no. 1, pp. 516–523, Jan. 2016.
- [7] Y. Zhengkun and Z. Yilei, "Recognizing tactile surface roughness with a biomimetic fingertip: A soft neuromorphic approach," *Neurocomputing*, vol. 244, no. Supplement C, pp. 102–111, 2017. [Online]. Available: <http://www.sciencedirect.com/science/article/pii/S0925231217305209>
- [8] U. B. Rongala, A. Mazzoni, and C. M. Oddo, "Neuromorphic artificial touch for categorization of naturalistic textures," *IEEE Trans. Neural Netw. Learn. Syst.*, vol. 28, no. 4, pp. 819–829, Apr. 2017.
- [9] S. Chun, Y. Choi, D. I. Suh, G. Y. Bae, S. Hyun, and W. Park, "A tactile sensor using single layer graphene for surface texture recognition," *Nanoscale*, vol. 9, pp. 10248–10255, 2017. [Online]. Available: <http://dx.doi.org/10.1039/C7NR03748A>
- [10] A. Khasnobish, M. Pal, D. N. Tibarewala, A. Konar, and K. Pal, "Texture-and deformability-based surface recognition by tactile image analysis," *Med. Biol. Eng. Comput.*, vol. 54, no. 8, pp. 1269–1283, 2016.
- [11] R. Li and E. H. Adelson, "Sensing and recognizing surface textures using a gelsight sensor," in *Proc. IEEE Conf. Comput. Vis. Pattern Recog.*, Jun. 2013, pp. 1241–1247.
- [12] W. Yuan, S. Dong, and E. H. Adelson, "Gelsight: High-resolution robot tactile sensors for estimating geometry and force," *Sensors*, vol. 17, no. 12, pp. 1–21, 2017. Art. no. 2762.
- [13] N. Jamali, P. Byrnes-Preston, R. Salleh, and C. Sammut, "Texture recognition by tactile sensing," in *Proc. Australasian Conf. Robot. Autom.*, Sydney, Australia, 2009, pp. 1–9.
- [14] N. Jamali and C. Sammut, "Material classification by tactile sensing using surface textures," in *Proc. IEEE Int. Conf. Robot. Autom.*, May 2010, pp. 2336–2341.
- [15] M. H. Evans, M. J. Pearson, N. F. Lepora, T. J. Prescott, and C. W. Fox, "Whiskered texture classification with uncertain contact pose geometry," in *Proc. IEEE/RSJ Int. Conf. Intell. Robots Syst.*, Oct. 2012, pp. 7–13.
- [16] M. H. Raibert and J. E. Tanner, "Design and implementation of a VLSI tactile sensing computer," *Int. J. Robot. Res.*, vol. 1, no. 3, pp. 3–18, 1982.
- [17] M. Shimojo, A. Namiki, M. Ishikawa, R. Makino, and K. Mabuchi, "A tactile sensor sheet using pressure conductive rubber with electrical-wires stitched method," *IEEE Sensors J.*, vol. 4, no. 5, pp. 589–596, Oct. 2004.
- [18] A. P. Gerratt, H. O. Michaud, and S. P. Lacour, "Elastomeric electronic skin for prosthetic tactile sensation," *Adv. Functional Mater.*, vol. 25, no. 15, pp. 2287–2295, 2015.
- [19] M. L. Hammock, A. Chortos, B. C. K. Tee, J. B. H. Tok, and Z. Bao, "25th anniversary article: The evolution of electronic skin (E-Skin): A brief history, design considerations, and recent progress," *Adv. Mater.*, vol. 25, pp. 5997–6038, 2013.
- [20] M. Pal, A. Khasnobish, A. Konar, D. N. Tibarewala, and R. Janarthanan, "Classification of deformable and non-deformable surfaces by tactile image analysis," in *Proc. Int. Conf. Control, Instrum., Energy Commun.*, Jan. 2014, pp. 626–630.
- [21] J. Sinapov, V. Sukhoy, R. Sahai, and A. Stoytchev, "Vibrotactile recognition and categorization of surfaces by a humanoid robot," *IEEE Trans. Robot.*, vol. 27, no. 3, pp. 488–497, Jun. 2011.
- [22] M. Rasouli, C. Yi, A. Basu, N. V. Thakor, and S. Kukreja, "Spike-based tactile pattern recognition using an extreme learning machine," in *Proc. IEEE Biomed. Circuits Syst. Conf.*, Oct. 2015, pp. 1–4.
- [23] D. Xu, G. E. Loeb, and J. A. Fishel, "Tactile identification of objects using Bayesian exploration," in *Proc. IEEE Int. Conf. Robot. Autom.*, 2013, pp. 3056–3061.
- [24] C. M. Oddo *et al.*, "Intraneural stimulation elicits discrimination of textural features by artificial fingertip in intact and amputee humans," *eLife*, vol. 5, Mar. 2016, Art. no. e09148.
- [25] C. M. Oddo, M. Controzzi, L. Beccai, C. Cipriani, and M. C. Carrozza, "Roughness encoding for discrimination of surfaces in artificial active-touch," *IEEE Trans. Robot.*, vol. 27, no. 3, pp. 522–533, Jun. 2011.
- [26] W. W. Lee, J. Cabibihan, and N. V. Thakor, "Bio-mimetic strategies for tactile sensing," in *Proc. IEEE Sensors*, Nov. 2013, pp. 1–4.
- [27] S. Datta, A. Khasnobish, A. Konar, D. N. Tibarewala, and R. Janarthanan, "Object shape and size recognition from tactile images," in *Proc. Int. Conf. Control Commun. Comput.*, Dec. 2013, pp. 16–21.
- [28] H. Liu, Y. Wu, F. Sun, and D. Guo, "Recent progress on tactile object recognition," *Int. J. Adv. Robot. Syst.*, vol. 14, no. 4, pp. 1–12, 2017.
- [29] S.-C. Liu and T. Delbruck, "Neuromorphic sensory systems," *Current Opin. Neurobiol.*, vol. 20, no. 3, pp. 288–295, 2010.
- [30] E. Neftci, J. Binas, U. Rutishauser, E. Chicca, G. Indiveri, and R. J. Douglas, "Synthesizing cognition in neuromorphic electronic systems," *Proc. Nat. Acad. Sci.*, vol. 110, no. 37, pp. E3468–E3476, 2013.
- [31] K. A. Boahen, "Point-to-point connectivity between neuromorphic chips using address events," *IEEE Trans. Circuits Syst. II, Analog Digit. Signal Process.*, vol. 47, no. 5, pp. 416–434, May 2000.
- [32] K. Boahen, "Neuromorphic microchips," *Sci. Am.*, vol. 292, no. 5, pp. 56–63, 2005.
- [33] M. Mahowald, "The silicon retina," in *An Analog VLSI System for Stereoscopic Vision*. New York, NY, USA: Springer, 1994, pp. 4–65.
- [34] G. Indiveri and R. Douglas, "Neuromorphic vision sensors," *Science*, vol. 288, no. 5469, pp. 1189–1190, 2000.
- [35] C. Brandli, R. Berner, M. Yang, S. C. Liu, and T. Delbruck, "A 240 latency global shutter spatiotemporal vision sensor," *IEEE J. Solid-State Circuits*, vol. 49, no. 10, pp. 2333–2341, Oct. 2014.
- [36] M. Pearson *et al.*, "A hardware based implementation of a tactile sensory system for neuromorphic signal processing applications," in *Proc. IEEE Int. Conf. Acoust., Speech, Signal Process.*, May 2006, vol. 4, pp. 1153–1156.
- [37] M. J. Pearson *et al.*, "Implementing spiking neural networks for real-time signal-processing and control applications: A model-validated FPGA approach," *IEEE Trans. Neural Netw.*, vol. 18, no. 5, pp. 1472–1487, Sep. 2007.
- [38] M. J. Pearson, B. Mitchinson, J. C. Sullivan, A. G. Pipe, and T. J. Prescott, "Biomimetic vibrissal sensing for robots," *Philosoph. Trans. Roy. Soc. London B: Biol. Sci.*, vol. 366, no. 1581, pp. 3085–3096, 2011.
- [39] E. K. Kim, S. A. Wellnitz, S. M. Bourdon, E. A. Lumpkin, and G. J. Gerling, "Force sensor in simulated skin and neural model mimic tactile SAI afferent spiking response to ramp and hold stimuli," *J. Neuroeng. Rehabil.*, vol. 9, no. 1, pp. 1–14, 2012. Art. no. 45.
- [40] S. S. Kim, A. P. Sripathi, R. J. Vogelstein, R. S. Armiger, A. F. Russell, and S. J. Bensmaia, "Conveying tactile feedback in sensorized hand neuroprostheses using a biofidelic model of mechanotransduction," *IEEE Trans. Biomed. Circuits Syst.*, vol. 3, no. 6, pp. 398–404, Dec. 2009.
- [41] L. L. Bologna, J. Pinoteau, R. Brasselet, M. Maggiali, and A. Arleo, "Encoding/decoding of first and second order tactile afferents in a neurorobotic application," *J. Physiology-Paris*, vol. 105, no. 13, pp. 25–35, 2011.
- [42] G. Spigler, C. M. Oddo, and M. C. Carrozza, "Soft-neuromorphic artificial touch for applications in neuro-robotics," in *Proc. IEEE RAS EMBS Int. Conf. Biomed. Robot. Biomechatronics*, 2012, pp. 1913–1918.
- [43] C. Eliasmith and C. H. Anderson, *Neural Engineering: Computation, Representation, and Dynamics in Neurobiological Systems*. Cambridge, MA, USA: MIT Press, 2004.
- [44] S. B. Furber *et al.*, "Overview of the SpiNNaker system architecture," *IEEE Trans. Comput.*, vol. 62, no. 12, pp. 2454–2467, Dec. 2013.
- [45] Y. Chen, E. Yao, and A. Basu, "A 128-channel extreme learning machine-based neural decoder for brain machine interfaces," *IEEE Trans. Biomed. Circuits Syst.*, vol. 10, no. 3, pp. 679–692, Jun. 2016.
- [46] G.-B. Huang, D. H. Wang, and Y. Lan, "Extreme learning machines: A survey," *Int. J. Mach. Learn. Cybern.*, vol. 2, no. 2, pp. 107–122, 2011.
- [47] A. Basu, S. Shuo, H. Zhou, M. H. Lim, and G.-B. Huang, "Silicon spiking neurons for hardware implementation of extreme learning machines," *Neurocomputing*, vol. 102, pp. 125–134, 2013.

- [48] L. Osborn, W. W. Lee, R. Kaliki, and N. Thakor, "Tactile feedback in upper limb prosthetic devices using flexible textile force sensors," in *Proc. 5th IEEE RAS/EMBS Int. Conf. Biomed. Robot. Biomechatronics*, Aug. 2014, pp. 114–119.
- [49] R. S. Johansson and A. B. Vallbo, "Tactile sensory coding in the glabrous skin of the human hand," *Trends Neurosci.*, vol. 6, pp. 27–32, 1983.
- [50] E. M. Izhikevich *et al.*, "Simple model of spiking neurons," *IEEE Trans. Neural Netw.*, vol. 14, no. 6, pp. 1569–1572, Nov. 2003.
- [51] A. Sahasranamam, I. Vlachos, A. Aertsen, and A. Kumar, "Dynamical state of the network determines the efficacy of single neuron properties in shaping the network activity," *Sci. Rep.*, vol. 6, May 2016, Art. no. 26029. [Online]. Available: <http://dx.doi.org/10.1038/srep26029>
- [52] B. S. Bhattacharya, C. Patterson, F. Galluppi, S. J. Durrant, and S. Furber, "Engineering a thalamo-cortico-thalamic circuit on spinnaker: A preliminary study toward modeling sleep and wakefulness," *Frontiers Neural Circuits*, vol. 8, 2014, Art. no. 46. [Online]. Available: <https://www.frontiersin.org/article/10.3389/fncir.2014.00046>
- [53] B. C.-K. Tee *et al.*, "A skin-inspired organic digital mechanoreceptor," *Science*, vol. 350, no. 6258, pp. 313–316, 2015.
- [54] G.-B. Huang, H. Zhou, X. Ding, and R. Zhang, "Extreme learning machine for regression and multiclass classification," *IEEE Trans. Syst., Man, Cybern. B, Cybern.*, vol. 42, no. 2, pp. 513–529, Apr. 2012.
- [55] C. Yi, E. Yao, and A. Basu, "A 128 channel 290 GMACs/W machine learning based co-processor for intention decoding in brain machine interfaces," in *Proc. IEEE Int. Symp. Circuits Syst.*, 2015, pp. 1–4.
- [56] A. Patil, S. Shen, E. Yao, and A. Basu, "Hardware architecture for large parallel array of random feature extractors applied to image recognition," *Neurocomputing*, vol. 261, pp. 193–203, 2017.
- [57] W. J. Ma and M. Jazayeri, "Neural Coding of Uncertainty and Probability," *Annu. Rev. Neurosci.*, vol. 37, pp. 205–220, 2014.
- [58] C. S. Wallace and D. M. Boulton, "An information measure for classification," *Comput. J.*, vol. 11, no. 2, pp. 185–194, 1968.
- [59] M. Gell-Mann and S. Lloyd, "Information measures, effective complexity, and total information," *Complexity*, vol. 2, no. 1, pp. 44–52, 1996.



Mahdi Rasouli received the B.Sc. degree in electrical and electronics engineering from Sharif University of Technology, Tehran, Iran, the M.Sc. degree from the Nanyang Technological University, Singapore, and the Ph.D. degree from the Graduate School for Integrative Sciences and Engineering, National University of Singapore.

Dr. Rasouli is a recipient of the Medtronic Industry Choice Award, which was presented to him at the IEEE International Conference on Biomedical Systems and Circuits in 2015.



Yi Chen received the B.Sc. degree in microelectronics from Xiamen University, Fujian, China, and the M.Sc. degree from the Chinese Academy of Science, Beijing, China, in 2007 and 2010, respectively, and the Ph.D. degree in electrical and electronic engineering from Nanyang Technological University, Singapore, in 2014.

He is currently with the Virtus IC Design Centre of Excellence as a Research Fellow. His research interest includes mainly analog front-end circuits design for sensor interfaces as well as low power mixed

signal machine learning IC design and system integration.



Sunil L. Kukreja received the B.S. degree in electrical and computer engineering from Johns Hopkins University, Baltimore, MD, USA, and the M.Eng. and Ph.D. degrees in biomedical engineering from McGill University, Montreal, QC, Canada.

He was a Postdoctoral Fellow with the Department of Electrical Engineering, Division of Automatic Control, Linköping University, Linköping, Sweden, from 2001 to 2002. From 2002 to 2004, he was with the McConnell Brain Imaging Center, Montreal Neurological Institute, Montreal, and the Federal Government in the USA from 2004 to 2014. He was a Principal Research Scientist with Singapore Institute for Neurotechnology, National University of Singapore, from 2014 to 2017.



Arindam Basu received the B.Tech and M.Tech degrees in electronics and electrical communication engineering from the Indian Institute of Technology, Kharagpur, in 2005, and the M.Sc. degree in mathematics and the Ph.D. degree in electrical engineering from the Georgia Institute of Technology, Atlanta, GA, USA, in 2009 and 2010, respectively. In June 2010, he joined Nanyang Technological University, Singapore, as an Assistant Professor. His research interests include bio-inspired neuromorphic circuits, non-linear dynamics in neural systems, low power

analog IC design, and programmable circuits and devices.

Dr. Basu received the JBNSTS Award in 2000 and the Prime Minister of India Gold Medal in 2005 from the Indian Institute of Technology, Kharagpur. He received the Best Student Paper Award, Ultrasonics Symposium, 2006; best live demonstration, ISCAS 2010; and a finalist position in the best student paper contest at ISCAS 2008. He was awarded MIT Technology Review's inaugural TR35@ Singapore award in 2012 for being among the top 12 innovators under the age of 35 in SE Asia, Australia, and New Zealand.



Nitish V. Thakor is currently a Professor of biomedical engineering with Johns Hopkins University, Baltimore, MD, USA, and the Director of the Singapore Institute for Neurotechnology, National University of Singapore, Singapore. His technical expertise is in the field of neuroengineering, where he has pioneered many technologies for brain monitoring to prosthetic arms and neuroprosthesis. He has authored more than 290 refereed journal papers, holds more than a dozen patents, and is the co-founder of three companies.

Dr. Thakor is a Fellow of the American Institute of Medical and Biological Engineering and the International Federation of Medical and Biological Engineering, and a Founding Fellow of the Biomedical Engineering Society. He is a recipient of a Research Career Development Award from the National Institutes of Health and a Presidential Young Investigator Award from the National Science Foundation. He is also a recipient of the Award of Technical Excellence in Neuroengineering from the IEEE Engineering in Medicine and Biology Society, the Distinguished Alumnus Award from IIT Bombay, Mumbai, India, and a Centennial Medal from the School of Engineering, University of Wisconsin–Madison, Madison, WI, USA.